ELSEVIER

Quaternary Science Reviews 25 (2006) 2806–2819

QSR

Reconstruction of the Grande Pile Eemian using inverse modeling of biomes and $\delta^{13}C$

D.D. Rousseau[a,b,c,*], Ch. Hatté[d,e], J. Guiot[f], D. Duzer[a], P. Schevin[a], G. Kukla[b]

[a]*Institut des Sciences de l'Evolution, Université Montpellier II, UMR CNRS-UM2 5554, case 61, place E. Bataillon, 34095 Montpellier cedex 05, France*
[b]*Lamont-Doherty Earth Observatory of Columbia University, Palisades, NY 10964, USA*
[c]*Universität Bayreuth, Lehrstuhl für Geomorphologie, 95447 Bayreuth, Germany*
[d]*Laboratoire des Sciences du Climat et de l'Environnement, UMR 1572 CEA/CNRS Bât 12, Domaine du CNRS, Avenue de la Terrasse, 91198 Gif sur Yvette Cedex, France*
[e]*NSF Arizona AMS laboratory, Physics building, PO Box 210081, Tucson, AZ 85721-0081, USA*
[f]*CEREGE, UMR 6635 CNRS/Université P. Cézanne, Europôle Méditerranéen de l'Arbois, BP 80-13545 Aix-en-Provence Cedex 04, France*

Received 26 September 2005; accepted 30 June 2006

Abstract

A new method to reconstruct past climatic conditions between 130 and 100 ka BP from pollen and isotopic data is applied to a previously unanalyzed Grande Pile core, GPXXI. We applied the inverse mode to the Biome4 vegetation model. The method utilizes $\delta^{13}C$, measured in parallel to the pollen samples as a constraint for the model. First the biomes and the $\delta^{13}C$ simulated by the model are compared with the biome allocation of the pollen data. The $\delta^{13}C$ to be simulated takes into account the degradation effect on the preserved organic matter. This procedure allows the reconstruction of the mean annual temperature and precipitation as well as the mean temperatures of the warmest and coldest months. We show that during the Eemian sensu stricto, the reconstructed precipitation is similar to modern values with low variability. The cold stadials and the penultimate glaciation are characterized by very low precipitation amounts. The temperature estimates, however, indicate differences with several oscillations identified. The peak values are reached at about 124–125 ka BP, but two other warm intervals are also identified. The variations in temperature appear to be related to sea-surface temperature oscillations in the North Atlantic region and are also in agreement with the timing of ice sheet build-up in the Northern Hemisphere. Seasonal variations are also identified in the estimated temperatures of the warmest and coldest months.

1. Introduction

The Eemian interval has long been considered the continental equivalent of marine substage 5e. Numerous ocean-continent comparisons were based on this correlation (Mangerud et al., 1979; Turon, 1984; Guiot et al., 1989; Sanchez Goni et al., 1999). However, the precise comparison of high-resolution marine and continental records clearly indicates that this is not the case. In fact, at least at middle and low latitudes, the terrestrial Eemian encompasses marine isotope substage 5e and part of 5d which corresponds to the first phase of ice build-up in high latitudes of the Northern Hemisphere (Kukla et al., 1997) (Fig. 1). This led to a debate about the duration of this interglacial sensu stricto (van Kolfschoten and Gibbard, 2000; Kukla et al., 2002a, b; McManus et al., 2002; Shackleton et al., 2002; Turner, 2002; Tzedakis et al., 2002). It now appears that steep vegetation and climate gradients occurred within the Eemian sensu lato at the inception of the ice build-up (Müller and Kukla, 2004). A comparison between the continental Eemian and marine isotope stratigraphy was made on marine core MD 95-2042 off Portugal in which a complete pollen sequence was retrieved in parallel with planktonic and benthic $\delta^{18}O$ stratigraphy (Shackleton et al., 2002). This analysis supports the main conclusion of the Grande Pile and VM

*Corresponding author. Institut des Sciences de l'Evolution, Université Montpellier II, UMR CNRS-UM2 5554, case 61, place E. Bataillon, 34095 Montpellier cedex 05, France. Tel.: +33 467 144 652; fax: +33 467 042 032.
E-mail addresses: denis@dstu.univ-montp2.fr, Denis.Rousseau@dstu.univ-montp2.fr (D.D. Rousseau).

0277-3791/$ - see front matter © 2006 Elsevier Ltd. All rights reserved.
doi:10.1016/j.quascirev.2006.06.011

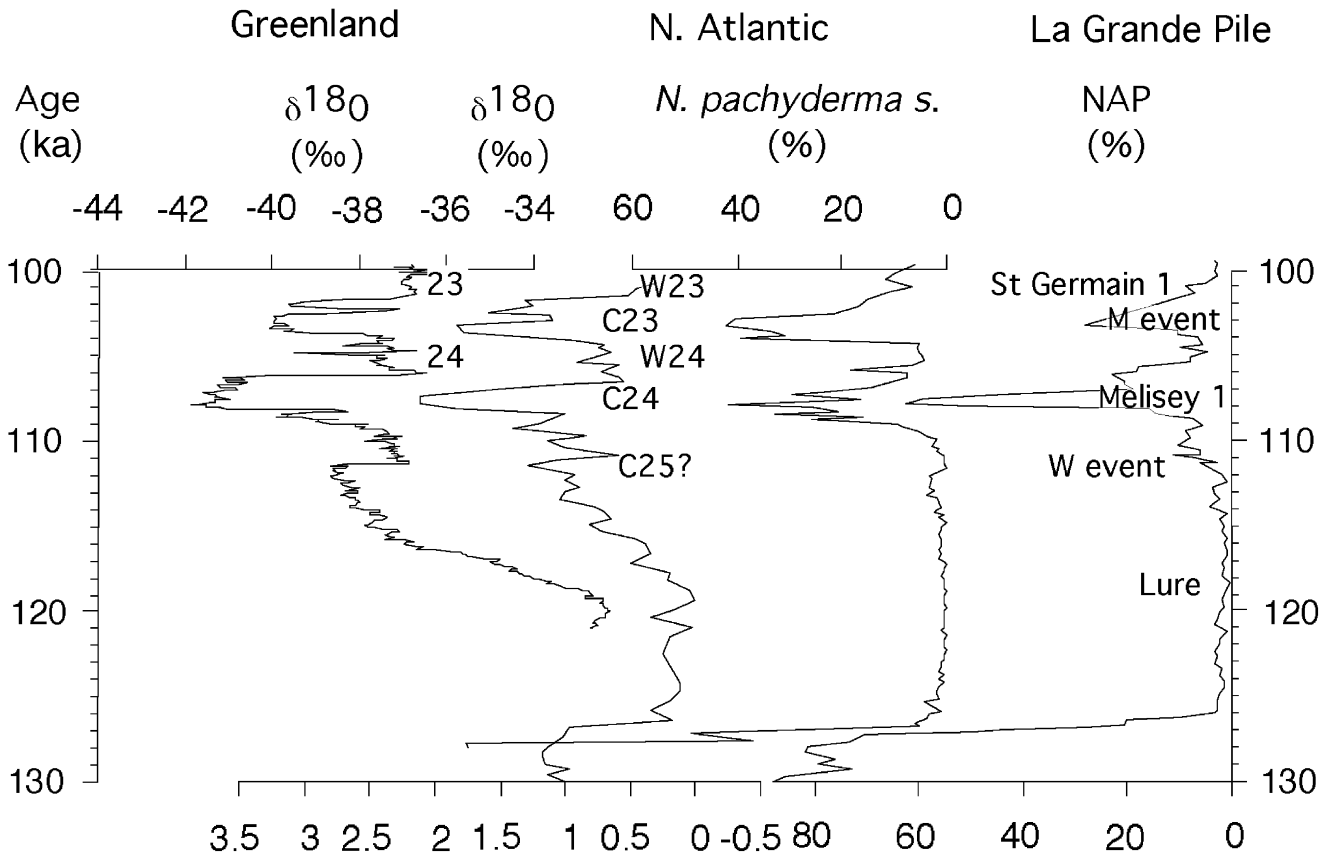

Fig. 1. Correlation between Greenland's $\delta^{18}O$ NorthGRIP record (North Greenland Ice Core Project Members, 2004), $\delta^{18}O$ and percent of *N. pachyderma* sinistral for North Atlantic core (MD95-2042, Shackleton et al., 2002) and percent non arboreal pollen for La Grande Pile (Woillard, 1978) climatic records between 130 and 100 ka BP modified after (Rousseau et al., 2006).

19-191 comparison showing that the continental Eemian sensu lato lasted longer than marine isotope substage 5e (Kukla et al., 1997). The correlation of different vegetation intervals with marine cold events was proposed earlier by McManus et al. (1994, 2002).

Numerous reconstructions of the environment or climate parameters have been proposed mostly based on the modern analog technique. These studies basically indicated little change during the Eemian (Guiot et al., 1989, 1997; Cheddadi et al., 1998; Klotz et al., 2003; Müller et al., 2003; Sanchez-Goni et al., 2005). However, these methods are calibrated on modern or sub-modern vegetation conditions mostly inferred from CO_2 concentrations, which did not prevail during the past. To address this limitation we use a new approach based on inverse modeling, which combines a palynological spectra and organic isotopic signature as forcings. This method is derived from the inverse modeling procedure used to reconstruct temperature and precipitation from pollen data (Guiot et al., 2000) and paleoprecipitation from the loess isotopic record (Hatté and Guiot, 2005). The output biome is constrained by temperature (seasonal distribution and mean annual value) and by the precipitation regime. $\delta^{13}C$ is added as a further constraining parameter in the inversion procedure resulting in improved limits to precipitation and consequently temperature ranges. However, the climatic signal of the isotopic signature of organic peat is much more complex than the $\delta^{13}C$ of loess organic matter. In a peat environment the organic matter originates from the complex mixture of biochemical components produced by the various organisms that lived in and around the bog. The composition of the mixture between algae and superior plants remains one of the major uncertainties that may be addressed by the organic carbon to total nitrogen (C_{org}/N_{tot}) ratio. Low C_{org}/N_{tot} values (<10) indicate that most of the sediment organic matter originates from algal production, whereas high values characterize a predominance of superior plant-fossilization (Meyers, 1994, 2003). Furthermore, the isotopic composition of the fossilized organic matter can differ from the original ^{13}C signature due to differential degradation of the biochemical components (lipids, amino acid etc.) and to the heterogeneous distribution of ^{13}C within biomolecules (Balesdent et al., 1993; van Bergen and Poole, 2002; Nguyen Tu et al., 2004; Poole et al., 2004). This remains one of the major topics in recent studies (van Bergen and Poole, 2002; Poole et al., 2004). Using inverse modeling Hatté et al. (2006) determined a likely mean isotopic shift of −1‰ for Grande Pile, which is in agreement with most reported studies (Adam et al., 1998; van Kaam-Peters et al., 1998; Pancost et al., 2003).

The aim of this paper is to develop a multiproxy approach by combining pollen data from GPXXI, $\delta^{13}C$ measurements and output from the Biome4 vegetation model to reconstruct in detail, the climate and environment for the last interglacial at the Grande Pile locality.

2. Materials and data

2.1. Pollen

The GPXXI core was retrieved at the Grande Pile site at the same time as those investigated by Woillard (1978; 1979a). It is presently preserved at the LDEO core repository. Grande Pile is located at 47°44′N, 6°30′E, 330 m a.s.l. with annual precipitation of 1080 mm and a mean annual temperature of 9.5 °C with a seasonal range of about 18 °C between the warmest and the coldest months (18.5–0.5 °C). The base of the core was investigated by measurements of the wet bulk density to define the occurrence of mineral versus organic intervals. This was used to define the main stratigraphical units such as the Linexert glaciation, the Lure interglacial, as well as the Eemian, Melisey and St Germain I biozones and the Montaigu event (Woillard, 1979b) (Fig. 2).

The sediment was sampled every 10 cm according to the bulk density record and covered the interval from 1830 to 1430 cm. Pollen samples were prepared as following: Defloculation of 0.2–0.5 g of sediment and humic acids dissolution by vigorous boiling in KOH 10%. Sieving under water of mineral or vegetal particles on a 180 μm mesh filter. Clay dissolution with HF 70% then HCl 20%. Final sample preparation by hot acetolysis with a mixture composed of 9/10 CH_3COOH and 1/10 H_2SO_4 and fuschin. Bottoms are diluted in glycerin (dilution by 10) and the material is prepared between plate and coverglass. The number of grains counted was also plotted against the number of taxa identified. The counting was stopped after a plateau was reached. The total number of grains counted varied from 82 in the mineral deposits at the base to more than 2000 in the organic samples. For the climate reconstruction, ferns and aquatic taxa have been removed, and the percentages recalculated.

The pollen biostratigraphy, shown in Fig. 2, indicates a complete record similar to those previously published (de Beaulieu and Reille, 1992; Woillard, 1978). The age model used in a previous interpretation of the Grande Pile record was applied to this record (Kukla et al., 1997) except for the age of the start of the Eemian which is taken as 128 ka BP (Shackleton et al., 2002; Rousseau et al, 2006). The assigned ages are shown in Fig. 3.

2.2. Biomisation of the pollen data

The biome definitions (Prentice et al., 1992) used in this study are updated as proposed in recent papers by Kaplan et al. (2003) and Bigelow et al. (2003), which improve the description of tundra vegetation. This is a better fit to the environment, especially for the cold conditions that we expect to reconstruct with the Biome4 vegetation model (Kaplan, 2001), compared to earlier definitions from Fauquette et al. (1999). The constituent plant functional types, defined according to physiological requirements (PFT), were applied to the pollen data. Supplemental Tables 1 and 2 list the assignment of pollen taxa to PFT,

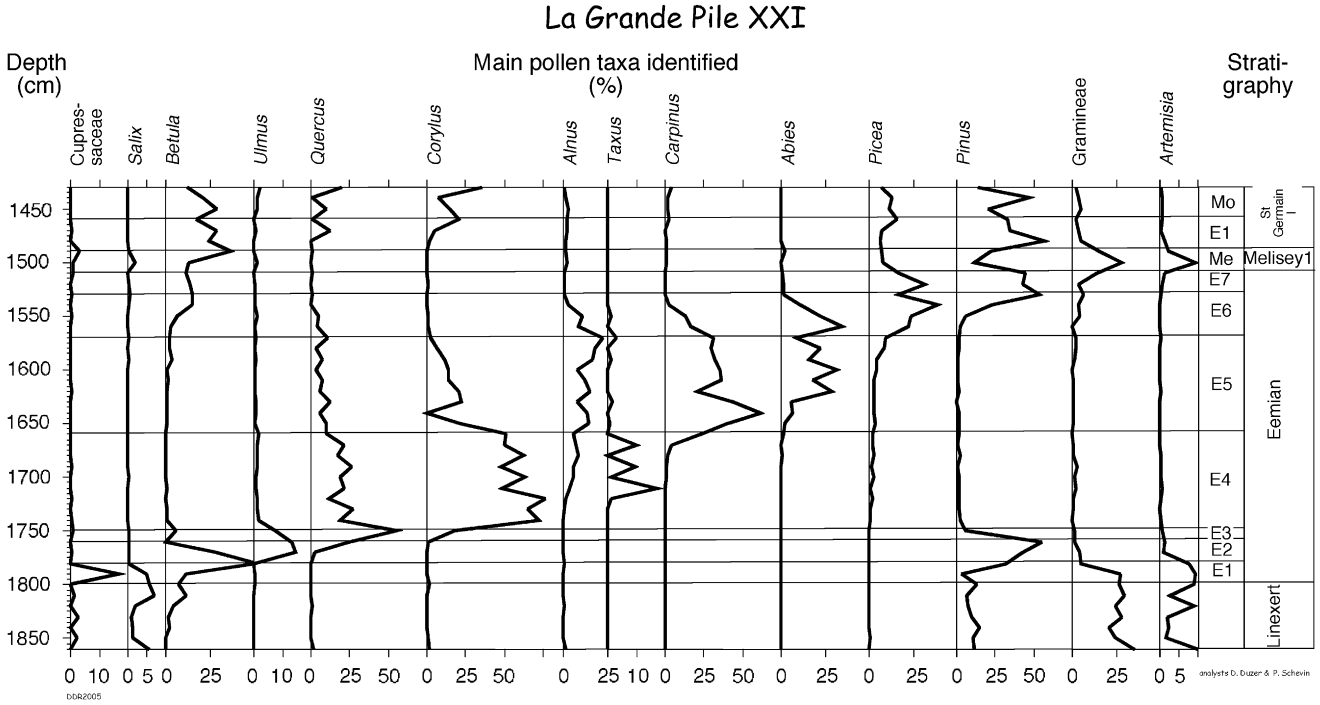

Fig. 2. Simplified pollen diagram of Grande Pile XXI core with the associated pollen biostratigraphy defined by Woillard (1978).

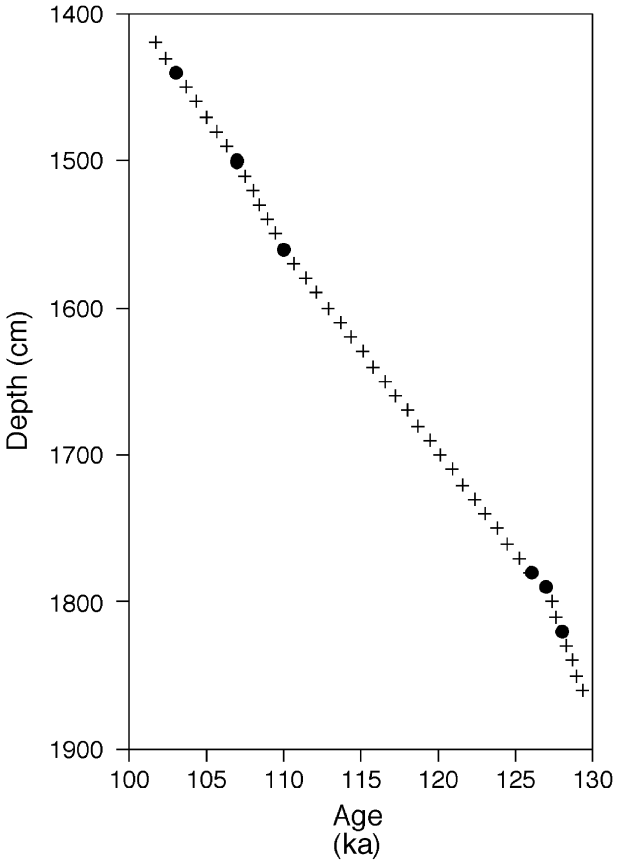

Fig. 3. Age model used for La Grande Pile core XXI with solid circles representing control ages (after Kukla et al., 1997; Rousseau et al. 2006; Shackleton et al., 2002). Ages interpolated between control points.

and the PFT to biomes. Every pollen sample is assigned to the most likely biome according to its affinity score following the biomisation protocol defined by Prentice et al (1996); every pollen taxon which contributes less than 0.5% to the pollen sum is excluded in the calculation of the affinity scores (Table 1). Some affinity scores are very close to each other suggesting several possible choices in the biome allocation (Table 1).

2.3. Carbon content and isotopic measurements

Samples were dried at 60 °C and leached with 4% HCl, rinsed, dried and homogenized. Total nitrogen, organic carbon contents were then determined with an Elementary Analyzer (EA-Vera Euro EA 3000), and isotopic ratios with the EA coupled with a dual inlet mass spectrometer (Micromass Optima). Isotopic results were obtained with a standard deviation of 0.2‰ allowing the interpretation of fluctuations higher than 0.6‰.

2.4. Biome4 vegetation model

Biome4 (Kaplan, 2001) is a process-based terrestrial biosphere model, modified from Biome3 (Haxeltine and Prentice, 1996) and includes an isotopic fractionation routine which was improved by Hatté and Guiot (2005). Model inputs include latitude, soil textural class, and monthly climate (temperature, precipitation and insolation) data. The model usually runs on a 0.5° grid, but can be run for any site with complete climate and soil data. Biome4 utilizes 13 potential PFTs representing the major bioclimatic types and growth forms of terrestrial plants. Association of PFTs allows the determination of a biome among 28 potential biomes. The Biome4 model includes a photosynthesis scheme that simulates acclimation of plants to external forcing by optimizing the net primary production (NPP) and the leaf area index (LAI). Additional rules to approximate the influence of light, canopy, fire risk, and snow are also included. To optimize NPP and LAI, taking into account external forcing, Biome4 uses a coupled carbon and water flux model. Competition among PFTs is simulated by using the optimal NPP of each PFT as an index of competitiveness. By comparing the optimized NPPs of every PFT, the Biome4 vegetation model determines the dominant, co-dominant, and grass-dominant (if different from the other two) PFTs. The model then determines the output biome from the successful PFTs, the corresponding NPP, respiration, gross primary production (GPP-respiration = NPP), and LAI. Fractionations by C3 and C4 plants are calculated using a model derived from Lloyd and Farquhar (1994). The mean annual isotopic fractionation is calculated by weighting monthly fractionation of C3 and C4 in all PFTs by the respective NPP. Biome4 then attributes the weighted isotopic fractionation to the output biome.

2.5. Inverse modeling

Here we use Biome4 in an inverse mode to reconstruct the most probable climate, starting from the outputs to infer some of the inputs of the model. We follow the procedure of Guiot et al. (2000), based on a Monte-Carlo sampling of monthly precipitation and temperature in a pre-defined range (Metropolis–Hastings algorithm (Hastings, 1970)).

In the inverse modeling process, some Biome4 inputs are known whereas others are unknown. The known inputs characterize the site and the related age-dependent parameters (i.e. soil type and texture, altitude, atmospheric CO_2 concentration and isotopic value). The soil parameters are defined according to the Food and Agriculture Organization (FAO) grid, and according to the vegetation to be simulated. The isotopic composition of atmospheric CO_2 is constant at −6.80‰, corresponding to a mean value measured for the Eemian (Schmitt and Fischer, 2005). The atmospheric CO_2 variation is based on that reported by Petit et al. (1999) and was resampled according to the Grande Pile time-scale. The unknown Biome4 inputs are climatic parameters such as precipitation and temperature (annual value and seasonal distribution) that need to be computed to fulfill the expected outputs. Finally, the target outputs are one or two pre-determined biomes by the pollen data, and the observed $\delta^{13}C$. The target biomes are

Table 1
Biome scores obtained for the GP XXI pollen spectra analyzed in this study

Bigelow	Biome4	1860	1850	1840	1830	1820	1810	1800	1790	1780	1770	1760	1750	1740	1730	1720
STEP	Step	16.55	11.28	7.47	11.88	15.59	10.99	17.03	14.61	4.76	3.28	0.96	1.40	0.00	0.40	0.59
CUSH	CuTund	15.24	12.43	6.94	11.88	13.28	9.58	15.87	12.83	4.76	3.28	0.96	1.40	0.00	0.40	0.00
DRYT	StTund	17.11	19.20	14.28	18.49	19.19	15.10	20.01	16.43	5.55	4.51	0.96	1.60	0.00	0.40	0.00
PROS	PShTund	17.51	13.27	7.77	12.45	14.43	12.15	18.16	14.92	4.76	3.28	0.96	1.40	0.00	0.40	0.00
DWAR	DShTund	15.15	13.37	14.87	14.09	14.98	19.43	16.49	16.30	9.99	8.48	0.00	3.35	0.00	0.40	0.00
SHRU	ShTund	14.38	10.67	12.59	11.89	13.12	20.84	16.33	20.59	14.99	17.25	0.00	5.22	0.00	0.56	0.91
CLDE	DeTaig	18.66	6.04	10.39	9.42	11.76	21.19	20.11	21.99	26.89	22.55	8.11	13.69	9.87	10.73	12.67
TAIG	EgTaig	18.66	6.36	10.39	9.42	11.76	21.19	20.11	21.99	26.89	22.55	8.11	13.69	9.87	11.00	13.85
COCO	CoCoFo	8.41	5.00	5.97	6.12	5.71	9.31	10.42	11.12	12.69	15.81	12.39	16.15	19.45	18.84	22.62
CLMX	ClMxFo	8.41	4.68	5.97	6.12	5.71	9.31	10.42	11.12	12.69	15.81	12.39	16.15	19.45	18.58	21.44
TEDE	TeDeFo	15.44	5.52	6.81	6.70	7.34	11.89	12.71	13.21	12.69	20.93	21.51	30.19	25.80	28.05	26.85
COMX	CoMxFo	13.54	5.84	6.81	6.70	7.34	11.89	12.71	13.21	12.69	17.20	17.28	23.57	23.77	24.61	25.98

Bigelow	Biome4	1710	1700	1690	1680	1670	1660	1650	1640	1630	1620	1610	1600	1590	1580	1570
STEP	Step	1.27	1.50	1.42	0.00	0.46	0.00	0.60	2.41	0.00	1.07	0.57	0.00	0.79	2.77	1.20
CUSH	CuTund	1.27	0.85	1.42	0.00	0.46	0.00	0.60	0.64	0.00	0.48	0.57	0.00	0.79	1.17	1.20
DRYT	StTund	1.95	0.85	1.59	0.00	0.46	0.00	1.31	0.64	0.22	0.48	1.29	0.00	1.22	1.65	2.00
PROS	PShTund	1.27	0.85	1.42	0.00	0.46	0.00	0.60	0.64	0.00	0.48	0.57	0.00	0.79	1.17	1.20
DWAR	DShTund	2.26	0.85	1.59	0.00	0.46	0.00	2.03	0.64	0.57	0.96	2.06	0.35	2.98	3.06	3.23
SHRU	ShTund	3.15	2.30	2.58	2.83	2.53	2.29	5.92	3.64	3.62	4.84	5.71	3.37	7.94	7.49	7.95
CLDE	DeTaig	14.36	15.79	14.41	17.64	14.66	14.89	18.90	12.05	13.77	18.54	17.06	13.41	21.11	20.19	20.02
TAIG	EgTaig	15.03	17.35	15.28	19.28	15.96	17.27	21.87	16.13	17.53	25.40	22.92	20.89	27.08	27.78	25.95
COCO	CoCoFo	22.32	22.52	21.91	23.54	23.90	26.66	25.85	19.80	26.75	31.32	28.58	29.99	29.90	29.02	26.08
CLMX	ClMxFo	21.65	20.95	21.04	21.90	22.60	24.29	22.88	15.73	22.99	24.47	22.73	22.51	23.93	21.43	20.15
TEDE	TeDeFo	31.49	30.54	32.61	33.49	34.29	35.15	36.67	28.28	34.09	30.13	33.14	30.07	35.43	30.00	34.11
COMX	CoMxFo	24.61	28.11	26.21	30.46	27.83	32.03	32.00	25.65	31.77	37.46	34.59	34.30	35.62	34.95	32.28

Bigelow	Biome4	1560	1550	1540	1530	1520	1510	1500	1490	1480	1470	1460	1450	1440	1430	1420
STEP	Step	2.02	1.90	2.49	2.46	2.01	4.88	12.99	6.55	3.04	1.84	3.51	2.42	2.66	1.20	1.25
CUSH	CuTund	0.00	1.90	1.84	2.46	2.81	4.88	10.98	6.30	3.04	1.84	1.28	2.42	2.66	1.20	1.25
DRYT	StTund	0.00	3.00	1.84	2.90	2.81	6.58	13.98	7.58	3.04	2.63	1.55	3.20	2.66	1.20	1.25
PROS	PShTund	0.00	1.90	1.84	2.69	2.81	4.88	12.18	6.30	3.04	1.84	1.28	2.42	2.66	1.20	1.49
DWAR	DShTund	1.55	5.40	5.64	7.64	5.42	8.73	17.64	11.10	7.08	7.98	5.69	8.16	6.30	4.64	3.13
SHRU	ShTund	6.02	9.12	9.11	10.49	7.90	10.14	22.46	15.83	10.70	12.68	9.78	12.99	9.85	7.40	4.60
CLDE	DeTaig	15.49	19.91	20.66	22.31	19.68	19.66	28.64	27.42	25.84	27.54	26.27	28.92	25.32	21.43	15.93
TAIG	EgTaig	26.01	29.40	30.08	27.32	26.35	23.72	31.39	31.40	28.33	30.11	30.20	32.20	28.86	24.02	20.22
COCO	CoCoFo	27.47	28.99	24.13	17.86	19.52	15.13	14.10	18.91	18.32	19.73	25.43	24.20	22.65	25.10	26.84
CLMX	ClMxFo	16.95	19.50	14.72	12.86	12.84	11.07	11.35	14.92	15.83	17.16	21.49	20.92	19.12	22.50	22.55
TEDE	TeDeFo	20.85	25.22	14.53	13.22	12.31	11.96	15.23	15.51	17.29	22.75	24.65	27.61	22.43	31.40	31.82
COMX	CoMxFo	32.29	33.44	25.64	19.17	20.05	16.01	16.50	20.49	19.19	24.35	27.10	28.77	24.11	30.05	29.64

STEP = STEP: temperate grassland/temperate xerophytic shrubland; CUSH = CuTund: cushion-forb tundra; DRYT = StTund: graminoid and forb tundra; PROS = PshTund: prostrate dwarf-shrib tundra; DWAR = DshTund: erect dwarf-shrub tundra; SHRU = ShTund: low- and high-shrub tundra; CLDE = DeTaig: cold deciduous forest; TAIG = EgTaig: cold evergreen needle-leaved forest; COCO = CoCoFo: cool evergreen needle-leaved forest; CLMX = ClMxFo: cool-temperate evergreen needle-leaved forest; TEDE = TeDeFo: temperate deciduous forest; COMX = CoMxFo: cool mixed forest (after Bigelow et al. (2003).

the two with the highest scores achieved by the biomisation procedure. Nevertheless, to remain close to the most probable vegetation, if the second score is lower than 90%, the best-scoring biome normally will be considered alone and thus as the unique constraint (Table 1). The Biome4 model consistently outputs Cool Mixed Forest (CoMxFo) and Steppe Tundra (StTund) (Bigelow et al., 2003). Thus if either vegetation type results as the unique constraining biome, a second biome was added as constraint even if its score was less than the 90% threshold. Four simulations with four series of target $\delta^{13}C$ were performed considering possible carbon isotopic fractionations linked to the microbial degradation. Shifts of −2‰, −1‰, 0‰ and +1‰ were considered in Hatté et al. (2006) where the −1‰ shift appeared to be the most likely for the main part of the studied sequence. This paper focuses on the simulation performed with an input vector considering this −1‰ isotopic shift.

The agreement between the modeled outputs and the observations is evaluated by the following equation:

$$D^2_{\text{isot}} = -\frac{(\delta^{13}C_o - \delta^{13}C_s)^2}{S^2}, \quad (1)$$

where subscripts 'o' and 's' correspond to target and simulated values respectively, and S^2 is the inverse of the residual variance, also called the precision of the estimates.

The calculation is made when the simulated biome matches one of the target biomes. Simulations providing a biome different from the two target biomes are rejected. The algorithm chooses between two of the input biomes to enhance its flexibility. Five parameters are used to maximize D^2: (i) January temperature, (ii) July temperature, (iii) January precipitation, (iv) July precipitation (the temperature and precipitation of the other months are calculated by sinusoidal interpolation between January and July), and (v) S^2 the model precision. Sunshine percentage is also an input of Biome4, and is estimated by linear regression from temperature and precipitation of the same month as described by Guiot et al. (2000).

The inversion process starts with random values for the five parameters taken from initial sampling intervals, and are defined as anomalies from a reference state. The required climatic variables (i.e. monthly precipitation, temperature, and cloudiness) are also estimated as anomalies. They are updated to new values according to the rules of the algorithm and a new run is performed. The probability distribution of the five input parameters is computed after several thousand iterations, while that of $\delta^{13}C$ is also calculated, and compared to the observed value to check the quality of the fit. All distributions are calculated within the 95%-confidence interval.

3. Results

3.1. C, N, and isotopic measurements (Table 2)

The C_{org}/N_{tot} values range from 11 to 25, and support the reliability of peat organic matter as mostly resulting from the degradation of superior vegetation and not from a mixture of aquatic and atmospheric contributions (at least for the levels above 1820 cm with a C/N higher than 15).

The carbon isotopic values range from −23.1 and −33.3‰, showing the presence of only C3 plants all along the studied interval. The heaviest values (> − 27‰) are obtained below 1750 cm, with the maxima (−23.1‰) at 1810 cm. The $\delta^{13}C$ slightly decreases from 1750 to 1550 cm to reach −33‰, followed by an enrichment of −27.8‰ at 1500 cm. Finally, the $\delta^{13}C$ decreases again to −33.3‰ at 1440 cm.

3.2. Pollen biostratigraphy and variability (Fig. 2)

The pollen stratigraphy is the same as initially described by Woillard (1978; 1979a) therefore her nomenclature and subdivisions are used.

The base of the record (1860–1800 cm) corresponds to mineral deposits, which yielded high proportions of Gramineae, and *Artemisia* indicating steppe conditions. This first zone corresponds to the Linexert glaciation.

A predominantly organic sediment record occurs between 1800 and 1510 cm. Seven intervals show the classical vegetation succession of an interglacial corresponding to the Lure-Eemian biozone. Zone E1 (1800–1780 cm) is composed of *Betula*, *Salix*, *Juniperus* and is representative of a tundra vegetation.

Zone E2 (1780–1760 cm) is the *Betula–Pinus* forest corresponding to a taiga with the occurrence of *Ulmus* on top.

Zone E3 (1760–1750 cm) is the *Quercetum-mixtum* forest corresponding to the warm temperate forest, which shows the classical succession described by Woillard with the occurrence of *Fraxinus*, even at percentages lower than 1%, in the mid part and *Corylus* on top.

Zone E4 (1750–1660 cm) is the *Corylus* forest characteristic of a warm temperate forest with three subdivisions and a maximum in *Taxus*.

Zone E5 (1660–1570 cm) is the *Carpinus* forest interpreted as the climatic optimum according to Woillard (1978).

Zone E6 (1570–1530 cm) consists of the development of a cold temperate forest identified by *Abies-Picea* and a main event identified at 1560 cm marked by the strong decrease in the deciduous trees compared to the needle leaved taxa (Woillard's event).

Zone E7 (1530–1510 cm) is the *Pinus–Picea–Betula* forest corresponding to a boreal forest, a taiga, with a climate change indicated in the following zone:

A silty clay horizon (1510–1490 cm) is characterized by steppe conditions indicated by high percentages of Gramineae, *Artemisia* and Chenopodiaceae. This corresponds to the Melisey I biozone characteristic of cold conditions.

A new organic interval starts (1490-1430) corresponding to the St. Germain I interstadial. At its base, a boreal forest consisting of *Pinus*, *Betula* and *Picea* characterize a taiga.

A separate event, detected by the analysis of the bulk-wet density, is identified at a depth of 1440 cm. It shows high values of *Pinus* and *Picea* contrary to the Melisey stadial, and is correlated with the Montaigu event.

The observed pollen biostratigraphy is identical to that described by Woillard (1978; 1979a) from earlier cores that she analyzed from Grande Pile, and were later studied by de Beaulieu and Reille (1992). This indicates that this new GPXXI record is complete even though the samples were taken at larger 10 cm intervals. It is sufficiently detailed for the presented climate reconstruction. The previously defined age model (Fig. 3) can-be applied to the pollen data in order to relate some of the pollen variability to other climate and environmental variations.

3.3. Variation of total arboreal (AP) and deciduous arboreal (DAP) percentages: a first indication of the vegetation changes (Fig. 4)

The AP percentages show only a few variations in the studied interval. Low values characterize the Linexert

Table 2
C, N and isotopic measurements for GP XXI

Depth (cm)	C/N	C (%)	N (%)	δ^{13}C (‰)	Target biome(s)		Simulated biome
1420				−32.10	TedeFo	CoMxFo	TedeFo
1430	19.029	19.263	1.0123	−30.22	TedeFo	CoMxFo	CoMxFo
1440				−33.29	EgTaig		EgTaig
1450	23.454	25.483	1.0865	−30.91	EgTaig		EgTaig
1460				−31.06	EgTaig		EgTaig
1470	18.145	14.527	0.8006	−29.80	EgTaig	DeTaig	EgTaig
1480				−29.61	EgTaig	DeTaig	EgTaig
1490	17.703	10.374	0.586	−30.03	EgTaig		EgTaig
1500				−27.80	EgTaig	DeTaig	EgTaig
1510	24.972	18.444	0.7386	−30.45	EgTaig		EgTaig
1520				−30.93	EgTaig		EgTaig
1530	18.735	27.537	1.4698	−31.25	EgTaig		EgTaig
1540				−31.42	EgTaig		EgTaig
1550	18.432	12.082	0.6555	−33.01	CoMxFo	EgTaig (1)	EgTaig
1560				−32.89	CoMxFo	CoCoFo (1)	CoMxFo
1570	22.672	25.384	1.1196	−30.29	TedeFo	CoMxFo	CoMxFo
1580				−30.88	CoMxFo		CoMxFo
1590	21.618	25.98	1.2018	−31.04	CoMxFo	TedeFo	TedeFo
1600				−29.05	CoMxFo		CoMxFo
1610	20.65	23.58	1.1419	−30.04	CoMxFo	TedeFo	CoMxFo
1620				−30.77	CoMxFo		CoMxFo
1630	24.305	24.392	1.0036	−29.42	TedeFo	CoMxFo	TedeFo
1640				−28.71	TedeFo	CoMxFo	TedeFo
1650				−29.08	TedeFo		TedeFo
1660	17.343	13.599	0.7841	−29.70	TedeFo	CoMxFo	CoMxFo
1670	18.301	23.932	1.3077	−29.24	TedeFo		TedeFo
1680				−29.76	TedeFo	CoMxFo	TedeFo
1690	19.641	22.326	1.1367	−29.05	TedeFo		TedeFo
1700				−29.57	TedeFo	CoMxFo	TedeFo
1710	18.56	19.726	1.0628	−28.55	TedeFo		TedeFo
1720				−28.16	TedeFo	CoMxFo	TedeFo
1730	19.776	23.666	1.1967	−27.58	TedeFo		TedeFo
1740				−26.28	TedeFo	CoMxFo	TedeFo
1750	18.763	15.723	0.838	−27.25	TedeFo		TedeFo
1760				−25.43	TedeFo		TedeFo
1770	15.801	11.625	0.7357	−26.58	DeTaig	EgTaig	EgTaig
1780				−27.12	DeTaig	EgTaig	EgTaig
1790	15.161	6.5452	0.4317	−24.50	DeTaig	EgTaig	EgTaig
1800				−24.93	DeTaig	EgTaig	EgTaig
1810	11.336	1.6018	0.1413	−23.13	DeTaig		EgTaig
1820				−25.63	StTund	ShTund (2)	ShTund
1830	11.074	1.814	0.1638	−27.14	StTund	ShTund (2)	ShTund
1840				−26.68	DshTund	ShTund (2)	ShTund
1850				−28.08	StTund	ShTund (2)	ShTund
1860				−25.18	DeTaig	EgTaig	EgTaig

Comparison of the most likely biomes allocated to the pollen data through the biomisation procedure with those reconstructed by the Biome4 vegetation model. DShTund: dwarf shrub tundra, ShTund: shrub tundra, StTund: steppe tundra, EgTaig: evergreen taiga, DeTaig: deciduous taiga, CoCoFo: cool coniferous forest, CoMxFo: cool mixed forest, TeDeFo: temperate deciduous forest.

glaciation. The arboreal percentages then increase very rapidly reaching a maximum at about 123 ka BP. The values then remain rather stable between 123 and 108 ka BP. A strong drop in AP percentage between 108 and 106 ka BP, corresponds to the Melisey I stadial. It is immediately followed by an interval with a stable and high percentage of AP, characteristic of the base of the St. Germain I interstadial.

DAP percentages show a more variable pattern than AP. The index increases in two major steps, the first between 128 and 126 ka BP and second between 124.5 and 122 ka BP. The highest value is reached at about 122.5 ka BP and is followed by a decrease of about 21% at about 121 ka BP, corresponding to the maximum occurrence of *Taxus* in zone E4 (Fig. 2). Between 120 and 115, DAP% remains high and stable. A decrease of about 12.8% occurs between 115 and 114.5 ka BP, followed by a plateau between 114.5 and 111 ka BP. A marked decrease of about 36% occurs between 111 and 108 ka BP. It is followed between 108 and 107 ka BP by the Melisey I stadial marked by a minimum value of 14%.

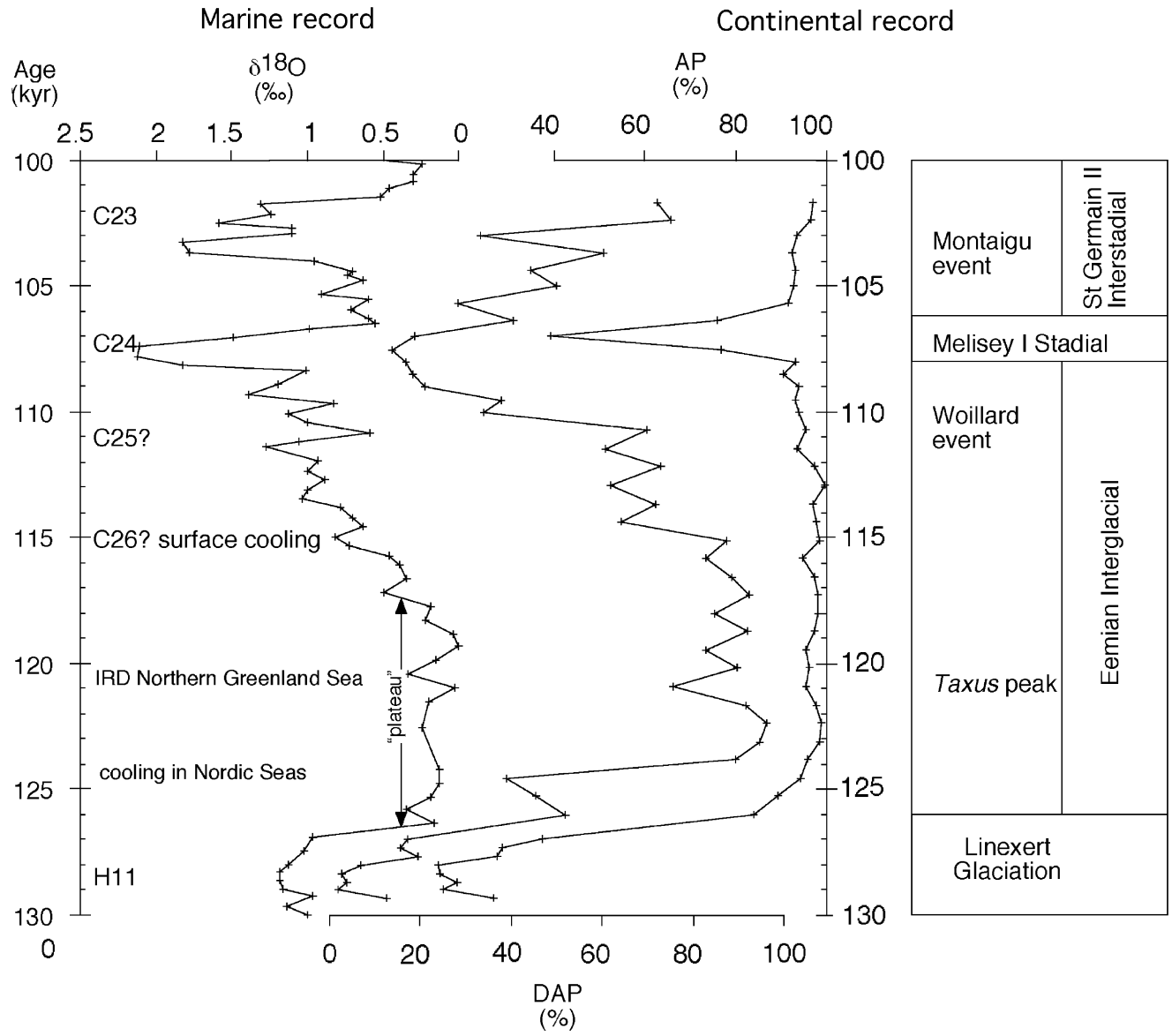

Fig. 4. Comparison of total arboreal pollen (AP) and temperate deciduous arboreal pollen (DAP) percentages in Grande Pile with the planktonic $\delta^{18}O$ variation from marine core MD 90-2042 (Shackleton et al., 2002). Pollen biostratigraphy according to Woillard (1978). Cold events related to iceberg discharges in the North Atlantic marked.

The St Germain I interstadial is marked by an increase from 43% to about 63% in DAP between 107 and 103.5 ka BP. This is interrupted by the low values (33%) of the Montaigu event at about 103 ka BP. High values of DAP% characterize the remaining stages of the St Germain I interstadial.

The disparity between the AP and DAP indices reflects their different composition. The AP% includes all types of arboreal vegetation including deciduous and needle leaved. Because of the low variation in AP% and the geographic location of the Grande Pile in the temperate part of Western Europe the DAP% provides more detail on the climate.

If our interpretation of the variability in the arboreal indices is correct, it should be reflected in the different estimates yielded by the Biome4 model. Mean annual temperature and precipitation (Tpann and Pann), mean temperatures of the coldest and warmest months (mtco and mtwa) are both expressed as anomalies from modern values.

3.4. Inverse modeling results (Figs. 5 and 6)

To take into account the uncertainty of the observations and measurements within the precision and the sensitivity of the model, we discuss the range of variation encompassed by the 95%-confidence interval rather than the "most probable value".

The inverse modeling procedure succeeds in simulating one of the two target biomes (Fig. 5) and yields isotopic

signatures in good agreement with the vegetation $\delta^{13}C$ deduced from the measurements (Fig. 5). Nevertheless, differences still remain at 103, 109.5, 110, 123.1, 124.5, and at levels older than 127 ka BP where the simulation yields heavier $\delta^{13}C$ than the presumed vegetation. Hatté et al. (2006) invoked an isotopic shift of higher magnitude (ca −2‰) at 103 ka BP, a bias due to the restricted ability of Biome4 to simulate CoMxFo in the 109.5–110 ka BP time-slice and better preservation of carbohydrates thanks to sulfurization inducing an enriched $\delta^{13}C$ degradation at 123.1, 124.5 and 127 ka BP. The levels older than 127.5 ka BP systematically show simulated $\delta^{13}C$ lighter than the target $\delta^{13}C$, but these levels are associated with low C_{org}/N_{tot} ratios and consequently can not be considered as resulting from the degradation of some single superior plants. Thus inverse-modeling results computed for samples older than 127.5 ka BP cannot be interpreted in terms of climatic change.

Among the four estimated climatic parameters, the mean annual temperature and the coldest and warmest month mean temperature anomalies are strongly dependent on the biome to be simulated, whereas the annual precipitation is strongly influenced by the $\delta^{13}C$ (Figs. 5, 6).

Prior to 125 ka BP the environmental conditions were dry and cold with the annual precipitation ranging from 300 to 500 mm yr^{-1} and a mean annual temperature of about 1 ± 2 °C. The very low annual mean temperature is mainly a product of the coldest month (mtco) indicating an anomaly of −19 to −24 °C compared to present, whereas the mtwa shows anomalies of −4 to +12 °C. This difference between the coldest and warmest month results in an enhanced seasonality which is ca 22 °C higher than today. This impacts the vegetation distribution by being unfavorable to tree growth (low DAP). Raising annual precipitation to ca 600 mm yr^{-1} which is comparable to the present associated with a *ca* 12 °C rise in all temperature parameters, leads to rapid improvement in the climatic conditions after about 125 ka BP. Nevertheless, the mtwa values are surprisingly high with a range of anomalies of 14.6–16.7 °C at 124.5 ka BP and 12.4–15.1 °C at

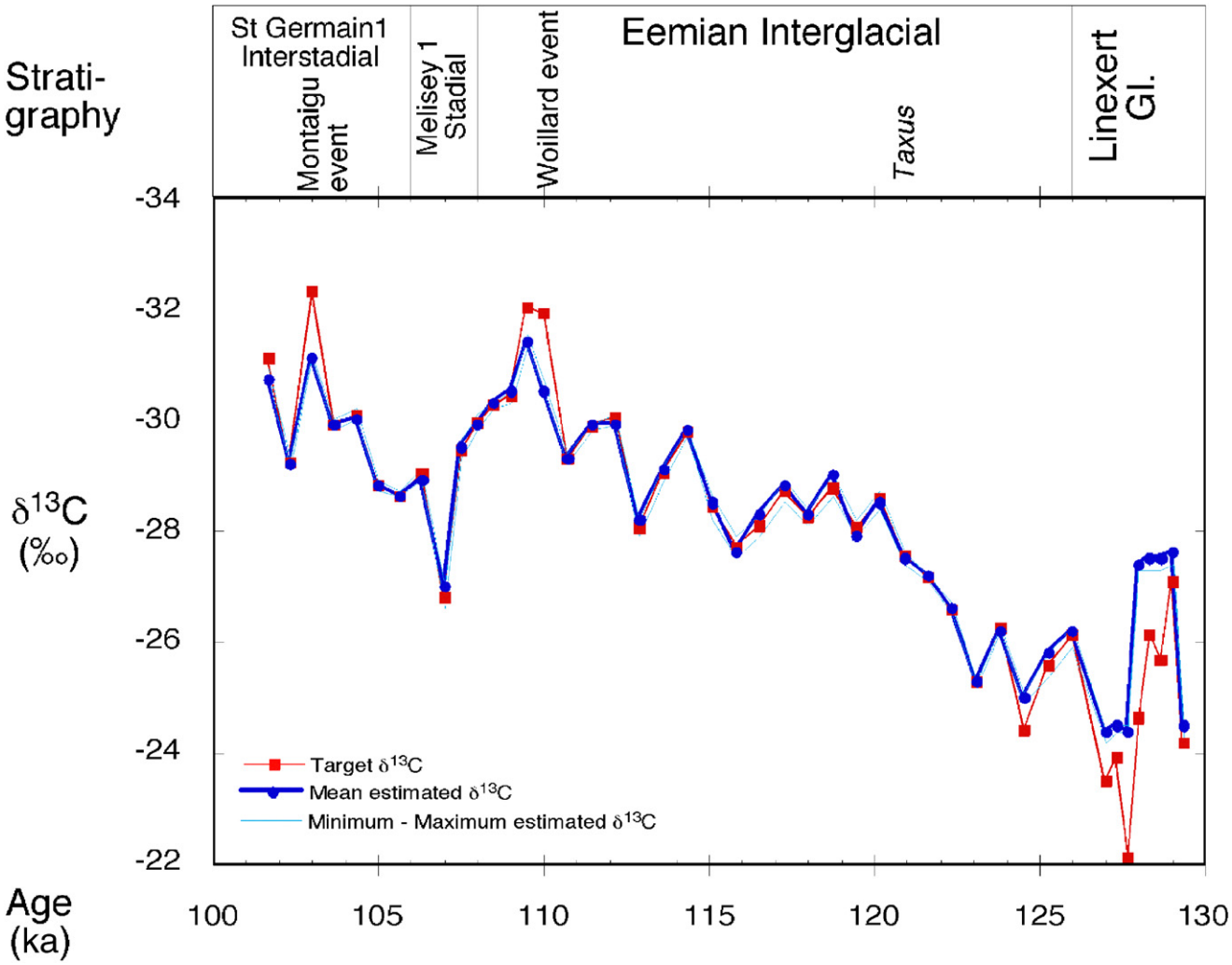

Fig. 5. Comparison of the estimated vegetation $\delta^{13}C$ derived from the measured $\delta^{13}C$, after considering a −1% degradation of the organic matter and the model simulated $\delta^{13}C$ for the 130 to 100 ka BP interval. The maximum and minimum estimated values are also indicated. Pollen biostratigraphy according to Woillard (1978).

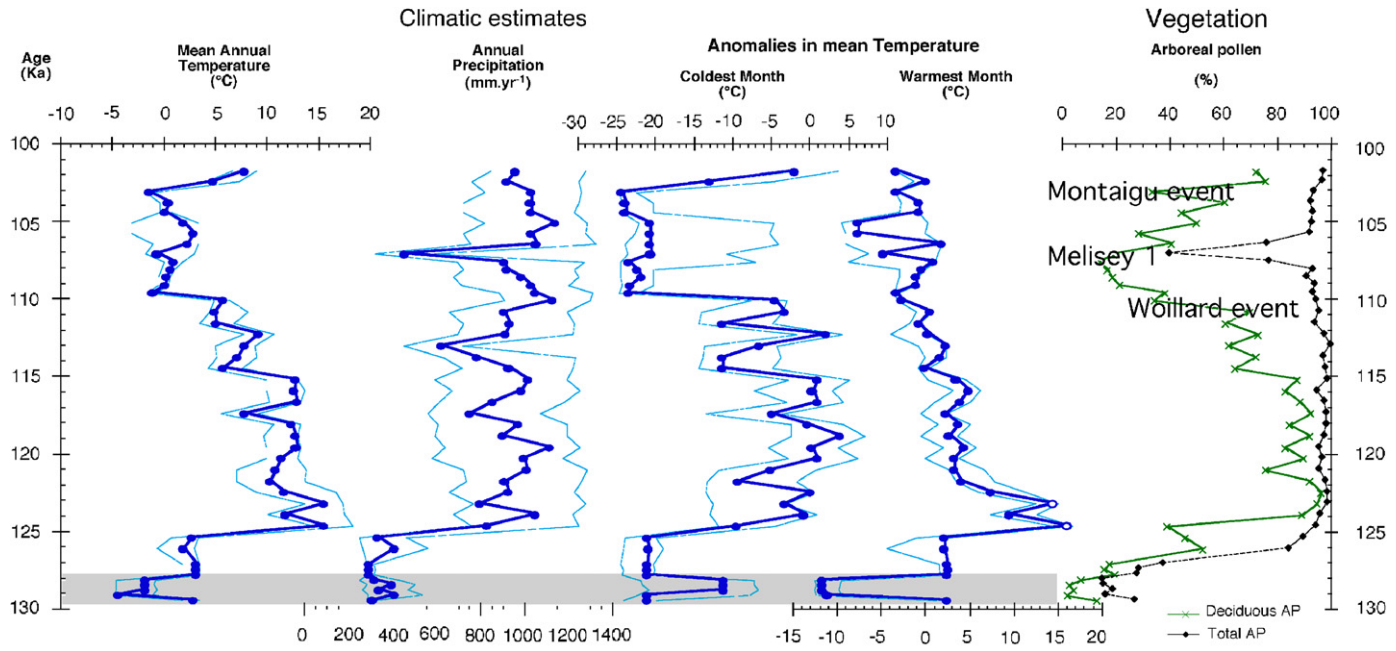

Fig. 6. Estimated climatic conditions from 130 to 100 ka BP based on model derived mean annual temperature and precipitation, coldest and warmest months mean annual anomalies compared to modern values. The heavy lines show the most probable values and the 95% confidence levels are marked by thin lines. The arboreal (x) and deciduous pollen (diamonds) variations are shown for Grande Pile XXI. The levels for which the C/N ratio prevents any reliable climatic reconstruction are highlighted in gray. Open circles for mean temperature of the warmest month indicates questionable values as described in the text.

123.1 ka BP. However, these two levels are among the four that Hatté et al. (2006) consider as indicating a possible bacterial degradation inducing isotope enrichment rather than a depletion (orange-colored sediment linked to carbohydrates sulfurization). In such an exceptional case of degradation, inverse modeling outputs mtwa anomaly ranges of 6.9–12.1 °C (7.8 °C as the most probable value) at 124.5 ka and 2.9–7.1 °C (3.0 °C as most probable), and no change in mtco and Pann, in addition to very small cooling for Tann. These values appear to be more realistic in the studied area but they do not weaken the return to milder conditions in a strong seasonality pattern. Indeed, seasonality is ca 9 °C higher than today between the coldest (absolute temperature ca −3 °C) and the warmest month (absolute temperature of ca 26 °C). The mean annual temperature remains stable until about 115 ka BP, then abruptly decreases by ca 6 °C reaching a plateau until 110 ka BP. This climate deterioration essentially resulted from colder, more variable mtco. It can be linked to the shift toward lower DAP. An abrupt decrease of ca 5 °C occurred between 110 and 109.5 ka BP. It was almost exclusively due to an 18 °C decrease of mtco and consequently led to increased seasonality that reached 40 °C between winter and summer. This strong change in the climate system was recorded by the vegetation, which changed abruptly from a deciduous to a more boreal taiga forest type. A relatively stable interval followed until about 103 ka BP. A high error margin is recorded at around 106 ka BP due the wide bioclimate of the simulated EgTaig associated with low $\delta^{13}C$ (Hatté et al., 2006). Given such a low values, the isotopic composition does not act as a determining constraint for the inverse modeling and does not succeed in narrowing the temperature and precipitation range. The mean annual temperature increases to about 9 °C after about 103 ka BP, once more resulting in a warmer winter. Subsequently at 125 ka BP, the annual precipitation remains constant. Two major decreases are identified at about 113 ka BP (ca 400 mm yr^{-1}) and at about 107 ka BP (ca 500 mm yr^{-1}).

4. Discussion

The comparison between our results and those from the North Atlantic cores (Fig. 7), e.g. NEAP18K (52°46′ N, 30°21′ W, 3275 m water depth), V29-191 (54°16′ N, 16°47′ W 2370 m water depth), ODP644 (66°40′ N, 4°34′ E, 1227 m water depth), HM71-19 (69°29′ N, 9°31′ W, 2210 m water depth), HM94-34 (73°46′ N, 2°32′ W, 1620 m water depth), HM52-43 (63°31′ N, 0°44′ E, 2781 m water depth), HM57-7 (68°26′ N, 13° 52’ W, 1620 m water depth) as well as the planktonic $\delta^{18}O$ of MD95-2042 (37°48′ N, 10°10′ W, 3148 water depth), in which the pollen record characterized the Eemian interglacial, (Shackleton et al., 2002) can provide additional information for the interpretation of the identified variations.

Very poor arboreal vegetation marks Heinrich event H11 (at 128–127 ka BP (Chapman and Shackleton, 1998; McManus et al., 1999, 2002; Tzedakis, 2003) at the base of the GP XXI record. The first Eemian warming at about 125 ka BP at La Grande Pile is shown in all temperature

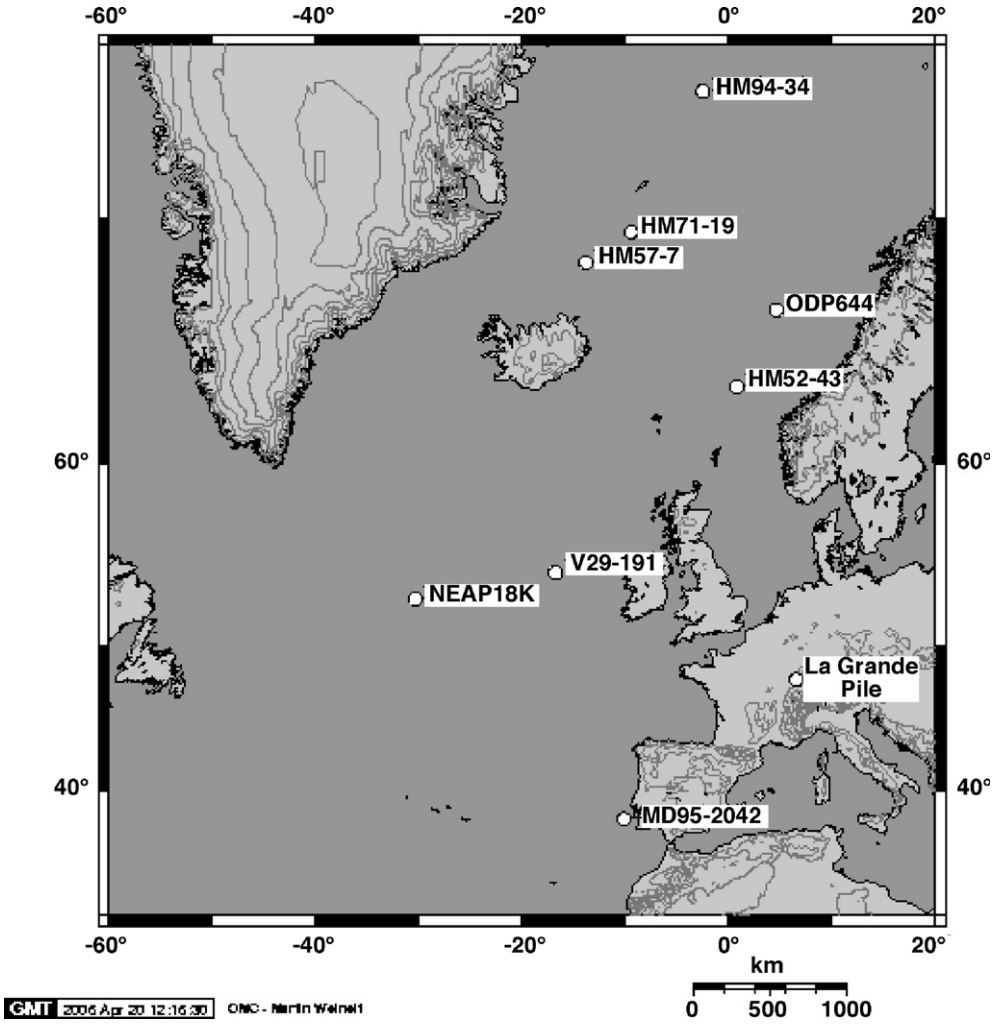

Fig. 7. Map indicating the location of the Grande Pile site and of the North Atlantic Ocean cores discussed in the text.

parameters (about 12 °C for the mean annual temperature), and is associated with a strong increase in annual precipitation (Fig. 6). This warming appears to have been strong in summer (19 °C) and in winter (20 °C) (Fig. 6). It could correspond to the northward migration of the polar front within the Greenland Sea described at 126–125 ka BP (Fronval and Jansen, 1996, 1997). An initial cooling at the land site occurs at about 124 ka BP, just after the interglacial optimum, indicated by a decreasing trend in DAP% and in all the temperature parameters. The mean annual precipitation signal does not show any particular trend. The variation in temperature is consistent with the first cooling in the Nordic Seas (Fronval et al., 1998), which corresponds to reduced influx in this region of Atlantic water and strong dominance of Arctic waters. Indeed, high-resolution records from the Norwegian Sea and Northeast Atlantic Ocean (Cortijo et al., 1994; Fronval and Jansen, 1996, 1997) indicate a sharp decrease in both temperature and salinity. This change in the thermohaline circulation in the Norwegian Sea may have been significant enough to be related to the cooling trend at Grande Pile. Starting at about 122 ka BP the mean temperature of the warmest month approached present day values. A second warming occurred between 120 and 118 ka BP, mainly expressed in the mtco month. The anomaly values remain negative and follow a small cold interval dated in our record between 123 and 121 ka BP. This event is marked by low values in DAP% during the *Taxus* peak (pollen zone E4, about 121 ka BP). This could correspond, considering the uncertainties of our age model, to the increase in IRD deposition recorded at about 122 ka BP in the northern Greenland Sea (Fronval et al., 1998) suggesting some freshwater flux input into the North Atlantic. This could affect zones of NADW production and potentially impact the neighboring continental vegetation (Fronval and Jansen, 1997).

The third Eemian warm interval at Grande Pile occurs between 116–118 ka BP and is mostly expressed in the annual and coldest month mean temperatures but only slightly in the mean temperature of the warmest month. The precipitation again does not show any particular trend in either the minimum or maximum estimates. This warm

interval matches the second warm interval during which the Arctic front reached its most westerly location in the Iceland Sea region (Fronval and Jansen, 1996, 1997).

A pronounced drop in mean annual as well as coldest and warmest month temperatures occurred at about 115 ka BP. It was associated with decreasing annual precipitation. A clear decrease in the deciduous trees marking the end of the interglacial sensu stricto in Grande Pile XXI following the maximum peak of *Carpinus* (pollen zone E5), took place at this time. Considering our limited time resolution, it may be related to the C26 cold event associated with a surface cooling in the North Atlantic. Indeed, in the northern North Atlantic core NEAP18K, the surface water temperature has been estimated to be almost cold as during the later C24 cold event (Chapman and Shackleton, 1999). The most prominent cooling of the surface water after the MIS 5e interval at 115 ka BP has been interpreted as the result of a dramatic change in the deep-water circulation (McManus et al., 2002; Shackleton et al., 2002).

The Woillard event (Kukla et al., 1997) refers to a rapid change in the composition of vegetation (Woillard, 1979b). The temperate hardwood forest, present at the locality since the beginning of the interglacial, was replaced, according to Woillard (1979b) by a boreal forest within 150 ± 75 yr. This is marked in Fig. 2 by the dominance of *Picea* over *Abies* associated with the decline of the temperate deciduous trees and by a decrease in the DAP%. It is a correlative of cool event C25, better expressed in northern North Atlantic cores, dated to about 111 ka BP (Chapman and Shackleton, 1999). IRD event C25 is interpreted as an advance of the Scandinavian, Svalbard-Barents and Greenland ice sheets surrounding the Nordic Seas. This event was also identified in the North Atlantic as the first large-scale cooling of the surface water after marine isotope stage 5e (Chapman and Shackleton, 1999; McManus et al., 1994, 2002; Shackleton et al., 2002). As described in Kukla et al (1997) the Melisey I stadial is correlative with the cool C24 event identified in the North Atlantic (McManus et al., 1994), and the Montaigu event corresponds to C23 (Fig. 4). Cold mean annual and coldest month temperatures are indicated between the Woillard event and the Melisey I stadial and are correlated to cold event C24. The Melisey I change in vegetation had been interpreted previously as a result of the IRD released in the North Atlantic following the first glacial inception. Indeed, the Melisey I stadial at about 107 ka BP is marked by low-temperature values and characterized by a strong decrease in annual precipitation of about 500 mm yr^{-1}. Precipitation remained high in the interval 110–107 ka BP while the mean annual and the coldest month temperatures were already very low. The decrease in precipitation lags the cooling by ca 3000 yr. The strong seasonality appears to be in agreement with the results of the 2D Earth Model of Intermediate Complexity (EMIC) MoBidiC which simulated the climate between 126 and 100 ka (Sanchez-Goni et al., 2005). The model indicates no continental ice in the Northern Hemisphere between 124 and 119 ka BP. Ice sheets then grow until 109 ka BP followed by partial melting until 104 ka BP. Our results indicate a decreasing trend in both mean annual and coldest month temperature from about 117 until the lowest values estimated at 110 ka BP. At about 106 ka BP a severe decrease in precipitation is indicated.

One of the main results of our investigation is that the climate of the last interglacial was not uniformly warm or wet. Our findings are in agreement with other continental, western European (Guiot et al., 1993; Thouveny et al., 1994; Klotz et al., 2004; Müller et al., 2005), and marine records (McManus et al., 1994; Fronval and Jansen, 1997; Fronval et al., 1998; Chapman and Shackleton, 1999; Shackleton et al., 2002), and could support the hypothesis of a modified thermohaline circulation during the Eemian affecting the climate on the western side of Europe (Broecker, 1998). However, the characterization of several pronounced coolings disagree with the interpretation of data from the same locality (Field et al., 1994; Cheddadi et al., 1998; Rioual et al., 2001) and off the Iberian peninsula (Sanchez-Goni et al., 2005) which show a relatively regular warm interval at about the same time.

5. Conclusion

The climate record of the GPXXI core parallels that of cores described earlier from the Grande Pile locality. In the interval between the Linexert Glaciation and the Montaigu event, i.e. between ca 130 and 100 ka BP, we tested a new method of producing climate reconstructions from pollen data, which differs from the direct use of analogs linked to modern vegetation conditions and modern CO_2 levels. The inverse mode of the biome vegetation model, constrained by $\delta^{13}C$ measured at the same levels as the pollen samples, allowed us to attempt a detailed reconstruction of climate conditions including the last interglacial, i.e., the Eemian sensu lato. Our investigation shows that the penultimate interglacial as defined at Grand Pile was characterized by numerous climate oscillations. The interglacial maximum occurred at about 125–124 ka BP and the strong cooling at about 111 ka BP is contemporaneous with the Woillard event characterizing a strong but rapid vegetation change leading to the disappearance of deciduous trees. A strong seasonality occurred as a result of different trends in the mean temperatures of the warmest and coldest months. Precipitation estimates do not indicate much variability during the Eemian except for a strong decrease at about 113 ka BP. The Linexert glaciation and the Melisey cold stadials are characterized by very low precipitation values of about 300 mm yr^{-1}, a deficit of about 700 mm yr^{-1} compare to modern values. Numerous other temperature fluctuations, mostly in the annual and coldest month mean temperatures, appear to be linked to surface temperature changes which occurred at the same time in the North Atlantic, linked to the building of the Northern Hemisphere ice-sheets. While the end of the oceanic MIS 5e

subzone, probably correlative with the demise of the Eemian sensu stricto in Northern Germany is very apparent in the vegetation changes at Grande Pile, the Eemian as defined here by the base of Melisey ended at about 108 ka BP B.P. and lasted approximately 20,000 years.

Acknowledgment

This study received a grant through the CNRS-NSF exchange program. The first author completed this paper during a stay at the University of Bayreuth thanks to a von Humboldt research award. Support provided by National Science Foundation Grants ATM-01-00830 and ATM-04-45038 to GK is appreciated. This is ISEM contribution 2006-029, LDEO contribution 6922 and LSCE contribution 1766. Sample material used in this project provided by the Lamont-Doherty Earth Observatory Deep-Sea Sample Repository. Support for the collection and curating facilities of the core collection is provided by the National Science Foundation through Grant OCE00-02380 and the Office of Naval Research through Grant N00014-02-1-0073. The inverse modeling method has been performed and tested thanks to a grant from the French PNEDC (VAGALAM project). Thanks to Joyce Gavin for editing the English, and to Cronis Tzedakis and an anonymous reviewer for very fruitful comments and suggestions.

Appendix A. Supplementary materials

Supplementary data associated with this article can be found in the online version at doi:10.1016/j.quascirev.2006.06.011.

References

Adam, P., Philippe, E., Albrecht, P., 1998. Photochemical sulfurization of sedimentary organic matter: a widespread process occurring at early diagenesis in natural environments? Geochimica et Cosmochimica Acta 62, 265–271.

Balesdent, J., Girardin, C., Mariotti, A., 1993. Site-related $\delta^{13}C$ of tree leaves and soil organic matter in a temperate forest. Ecology 74, 1713–1721.

Bigelow, N.H., Brubaker, L.B., Edwards, M.E., Harrison, S.P., Prentice, I.C., Anderson, P.M., Andreev, A.A., Bartlein, P.J., Christensen, T.R., Cramer, W., Kaplan, J.O., Lozhin, A.V., Matveyeva, N.V., Murray, D.F., McGuire, A.D., Razzhivin, V.Y., Ritchie, J.C., Smith, B., Walker, D.A., Gajewski, K., Wolf, V., Holmqvist, B.H., Igarashi, Y., Kremenetskii, K., Paus, A., Pisaric, M.F.J., Volkova, V.S., 2003. Climate change and artic ecosystems: 1. Vegetation changes north of 55°N between the last glacial maximum, mid-Holocene, and present. Journal of Geophysical Research 108, 8170.

Broecker, W.S., 1998. The end of the present interglacial: how and when? Quaternary Science Reviews 17, 689–694.

Chapman, M.R., Shackleton, N.J., 1998. Millennial-scale fluctuations in North Atlantic heat flux during the last 150,000 years. Earth and Planetary Science Letters 159, 57–70.

Chapman, M.R., Shackleton, N.J., 1999. Global ice-volume fluctuations, North Atlantic ice-rafting events, and deep-ocean circulation changes between 130 and 70 ka. Geology 27, 795–798.

Cheddadi, R., Mamakowa, K., Guiot, J., de Beaulieu, J.L., Reille, M., Andrieu, V., Granoszewski, W., Peyron, O., 1998. Was the climate of the Eemian stable? A quantitative climate reconstruction from seven European pollen records. Palaeogeography, Palaeoclimatology, Palaeoecology 143, 73–85.

Cortijo, E., Duplessy, J.C., Labeyrie, L., Leclaire, H., Duprat, J., Van Weering, T.C.E., 1994. Eemian cooling in the Norwegian Sea and North Atlantic Ocean preceding continental ice-sheet growth. Nature 372, 446–449.

de Beaulieu, J.L., Reille, M., 1992. The last climatic cycle at La Grande Pile (Vosges, France) a new pollen profile. Quaternary Science Reviews 11, 431–438.

Fauquette, S., Guiot, J., Menut, M., de Beaulieu, J.L., Reille, M., Guenet, P., 1999. Vegetation and climate since the last interglacial in the Vienne area (France). Global and Planetary Change 21, 1–17.

Field, M.H., Huntley, B., Müller, H., 1994. Eemian climate fluctuations observed in a European pollen record. Nature 371, 779–783.

Fronval, T., Jansen, E., 1996. Rapid changes in ocean circulation and heat flux in the Nordic seas during the last interglacial period. Nature 383, 806–810.

Fronval, T., Jansen, E., 1997. Eemian and early Weichselian (140–60 ka) paleoceanography and paleoclimate in the Nordic seas with comparisons to Holocene conditions. Paleoceanography 12, 443–462.

Fronval, T., Jansen, E., Haflidason, H., Sejrup, H.P., 1998. Variability in surface and deep water conditions in the Nordic Seas during the Last Interglacial period. Quaternary Science Reviews 17, 963–985.

Guiot, J., 1997. Back at the last interglacial. Nature 388, 25–26.

Guiot, J., de Beaulieu, J.L., Cheddadi, R., David, F., Ponel, P., Reille, M., 1993. The climate in Western Europe during the last glacial/interglacial cycle derived from pollen and insect remains. Palaeogeography, Palaeoclimatology, Palaeoecology 103, 73–93.

Guiot, J., Pons, A., de Beaulieu, J.L., Reille, M., 1989. A 140,000 year climatic reconstruction from two European pollen records. Nature 338, 309–313.

Guiot, J., Torre, F., Jolly, D., Peyron, O., Boreux, J.J., Cheddadi, R., 2000. Inverse vegetation modeling by Monte Carlo sampling to reconstruct palaeoclimates under changed precipitation seasonality and CO_2 conditions: application to glacial climate in mediterranean region. Ecological Modelling 127, 119–140.

Hastings, W.K., 1970. Monte-Carlo sampling methods using Markov chains and their application. Biometrika 57, 97–109.

Hatté, C., Guiot, J., 2005. Paleoprecipitation reconstruction by inverse modeling using the isotopic signal of loess organic matter: application to the Nußloch loess sequence (Rhine Valley, Germany). Climate Dynamics 25, 315–327.

Hatté, C., Rousseau, D.D., Guiot, J., Kukla, G., 2006. Shift in original isotopic signature of plants dure to degradation and paleoclimatic implications: contribution of the modeling. Global Biogeochemical Cycles, submitted for publication.

Haxeltine, A., Prentice, I.C., 1996. BIOME 3: an equilibrium terrestrial biosphere model based on ecophysiological constraints, resource availability and competition among plant functional types. Global Biogeochemical Cycles 10 (4), 693–709.

van Kaam-Peters, H.M.E., Schouten, M.R., Koster, J., Sinninghe Damsté, J.S., 1998. Controls on the molecular and carbon isotopic composition of organic matter deposited in a Kimmeridgian euxinic shelf sea: evidence for preservation of carbohydrates through sulfurization. Geochimica et Cosmochimica Acta 62, 3259–3283.

Kaplan, J.O., 2001. Geophysical applications of vegetation modeling. Unpublished Ph.D. thesis, Lund University.

Kaplan, J.O., Bigelow, N.H., Prentice, I.C., Harrison, S.P., Bartlein, P.J., Christensen, T.R., Cramer, W., Matveyeva, N.V., McGuire, A.D., Murray, D.F., Razzhivin, V.Y., Smith, B., Walker, D.A., Anderson, P.M., Andreev, A.A., Brubaker, L.B., Edwards, M.E., Lozhkin, A.V., 2003. Climate change and Arctic ecosystems: 2; modeling, paleodata-model comparisons, and future projections. Journal of Geophysical Research 108, 8171.

Klotz, S., Guiot, J., Mosbrugger, V., 2003. Continental European Eemian and early Würmian climate evolution: comparing signals using different quantitative reconstruction approaches based on pollen. Global and Planetary Change 36, 277–294.

Klotz, S., Müller, U.G., Mosbrugger, V., de Beaulieu, J.L., Reille, M., 2004. Eemian to early Würmian climate dynamics: history and pattern of changes in central Europe. Palaeogeography, Palaeoclimatology, Palaeoecology 211, 107–126.

Kukla, G., McManus, J.F., Rousseau, D.D., Chuine, I., 1997. How long and how stable was the last interglacial? Quaternary Science Reviews 16, 605–612.

Kukla, G.J., Bender, M.L., de Beaulieu, J.L., Bond, G., Broecker, W.S., Cleveringa, P., Gavin, J.E., Herbert, D., Imbrie, J., Jouzel, J., Keigwin, L.D., Knudsen, K.L., McManus, J.F., Merkt, J., Muhs, D., Müller, H., Poore, R.Z., Porter, S.C., Seret, G., Shackleton, N.J., Turner, C., Tzedakis, P.C., Winograd, I.J., 2002a. Last interglacial climates. Quaternary Research 58, 2–13.

Kukla, G.J., de Beaulieu, J.L., Svobodova, H., Andrieu-Ponel, V., Thouveny, N., Stockhausen, H., 2002b. Tentative correlation of pollen records of the last interglacial at Grande Pile and Ribains with marine isotope stages. Quaternary Research 58, 32–35.

Lloyd, J., Farquhar, G.D., 1994. ^{13}C discrimination during CO_2 assimilation by the terrestrial biosphere. Oecologia 99, (201-215).

Mangerud, J., Sonstegaardt, E., Sejrup, H.P., 1979. Correlation of the Eemian (interglacial) stage and the deep-sea oxygen-isotope stratigraphy. Nature 277, 189–192.

McManus, J.F., Bond, G.C., Broecker, W.S., Johnsen, S., Labeyrie, L., Higgins, S., 1994. High-resolution climate records from the North Atlantic during the last interglacial. Nature 371, 326–329.

McManus, J.F., Oppo, D.W., Cullen, J.L., 1999. A 0.5-million-year record of millennial-scale climate variability in the North Atlantic. Science 283, 971–975.

McManus, J.F., Oppo, D.W., Keigwin, L.D., Cullen, J.L., Bond, G.C., 2002. Last interglacial and prolonged interglacial warmth in the North Atlantic. Quaternary Research 58, (17–21).

Meyers, P.A., 1994. Preservation of elemental and isotopic source identification of sedimentary organic matter. Chemical Geology (Isotope Geoscience Section) 114, 289–302.

Meyers, P.A., 2003. Applications of organic geochemistry to paleolimnological reconstructions: a summary of examples from the Laurentian Great Lakes. Organic Geochemistry 34, 261–289.

Müller, U.G., Klotz, S., Geyh, M.A., Pross, J., Bond, G.C., 2005. Cyclic climate fluctuations during the last interglacial in central Europe. Geology 33, 449–452.

Müller, U.C., Kukla, G.J., 2004. North Atlantic current and European environments during the declining stage of the last interglacial. Geology 32, 1009–1012.

Müller, U.C., Pross, J., Bibus, E., 2003. Vegetation response to rapid climate change in Central Europe during the past 140,000 yr based on evidence from the Füramoos pollen record. Quaternary Research 59, 235–245.

Nguyen Tu, T.T., Derenne, S., Largeau, C., Bardoux, G., Mariotti, A., 2004. Diagenesis effects on specific carbon isotope composition of plant *n*-alkanes. Organic Geochemistry 35, 317–329.

North Greenland Ice Core Project Members, 2004. High-resolution record of Northern Hemisphere climate extending into the last interglacial period. Nature 431, 147–151.

Pancost, R.D., Baas, M., van Geel, B., Sinninghe Damste, J.S., 2003. Response of ombrotrophic bog to a regional climate event revealed by macrofossil, molecular and carbon isotopic data. The Holocene 13, 921–932.

Petit, J.R., Jouzel, J., Raynaud, D., Barkov, N.I., Barnola, J.-M., Basile, I., Bender, M., Chappellaz, J., Davis, M., Delaygue, G., Delmotte, M., Kotlyakov, V.M., Legrand, M., Lipenkov, V., Lorius, C., Pépin, L., Ritz, C., Saltzman, E., Stievenard, M., 1999. Climate and atmospheric history of the past 420,000 years from the Vostok ice core, Antarctica. Nature 399, 429–436.

Poole, I., van Bergen, P.F., Kool, J., Schouten, S., Cantrill, D.J., 2004. Molecular isotopic heterogeneity of fossil organic matter: implications for δ13C biomass and δ13C palaeoatmosphere proxies. Organic Chemistry 35, 1261–1274.

Prentice, I.C., Cramer, W., Harrison, S., Leemans, R., Monserud, R.A., Solomon, A.M., 1992. A global biome model based on plant physiology and dominance, soil properties and climate. Journal of Biogeography 19, 117–134.

Prentice, I.C., Guiot, J., Jolly, D., Cheddadi, R., 1996. Reconstructing biomes from palaeoecological data: a general method and its application to European pollen data at 0 and 6 ka. Climate Dynamics 12, 185–194.

Rioual, P., Andrieu-Ponel, V., Rietti-Shati, M., Battarbee, R.W., de beaulieu, J.L., Cheddadi, R., Reille, M., Svobodova, H., Shemesh, A., 2001. High-resolution record of climate stability in France during the last interglacial period. Nature 413.

Rousseau, D.D., Kukla, G., McManus, J., 2006. What is what in the ice and the ocean? Quaternary Science Reviews, 25, 2025–2030.

Sanchez Goni, M.F., Eynaud, F., Turon, J.L., Shackleton, N.J., 1999. High resolution palynological record off the Iberian margin: direct land-sea correlation for the Last Interglacial complex. Earth and Planetary Science Letters 171, 123–137.

Sanchez-Goni, M.F., Loutre, M.F., Crucifix, M., Peyron, O., Santos, L., Duprat, J., Malaize, B., Turon, J.L., Peypouquet, J.P., 2005. Increasing vegetation and climate gradient in Western Europe over the Last Glacial Inception (122–110 ka): data-model comparison. Earth and Planetary Science Letters 231, 111–130.

Schmitt, J., Fischer, H., 2005. A new micro sublimation technique for high-precision $\delta^{13}CO2$ analysis of ice cores: Instrumental set-up and first results. In: DEKLIM: The Climate of the Next Millennia in the Perspective of Abrupt Climate Change During the Late Pleistocene. University of Mainz, Mainz.

Shackleton, N.J., Chapman, M., Sanchez-Goni, M.F., Pailler, D., Lancelot, Y., 2002. The classic marine isotope substage 5e. Quaternary Research 58, 14–16.

Thouveny, N., de Beaulieu, J.L., Bonifay, E., Creer, K.M., Guiot, J., Icole, M., Johnsen, S., Jouzel, J., Reille, M., Williams, T., Williamson, D., 1994. Climate variations in Europe over the past 140 Kyr BP deduced from rock magnetism. Nature 371, 503–506.

Turner, C., 2002. Problems of the duration of the Eemian interglacial in Europe North of the Alps. Quaternary Research 58, 45–48.

Turon, J.L., 1984. Direct land/sea correlations in the last interglacial complex. Nature 309, 673–676.

Tzedakis, C., 2003. Timing and duration of Last Interglacial conditions in Europe: a chronicle of a changing chronology. Quaternary Science Reviews 22, 763–768.

Tzedakis, P.C., Frogley, M.R., Heaton, T.H.E., 2002. Duration of Last Interglacial conditions in Northwestern Greece. Quaternary Research 58, 53–55.

van Bergen, P.F., Poole, I., 2002. Stable carbon isotopes wood: a clue of palaeoclimate? Palaeogeography, Palaeoclimatology, Palaeoecology 182, 31–45.

van Kolfschoten, T., Gibbard, P.L., 2000. The Eemian-local sequences, global perspectives: introduction. Geologie en Mijnbouw 79, 129–133.

Woillard, G., 1978. Grande Pile peat bog: a continuous pollen record for the last 140,000 years. Quaternary Research 9 (1–XXI).

Woillard, G., 1979a. The Last Interglacial–Glacial cycle at Grande Pile in northeastern France. Bulletin de la Société belge de Géologie 88, 51–69.

Woillard, G.M., 1979b. Abrupt end of the Last Interglacial s.s. in northeast France. Nature 281, 558–562.